APRIL 01 2006

Sound generated by vortices in the presence of a porous half-cylinder mounted on a rigid plane

C. K. Lau; S. K. Tang

J. Acoust. Soc. Am. 119, 2084–2095 (2006)
https://doi.org/10.1121/1.2171838

Sound generated by vortices in the presence of a porous half-cylinder mounted on a rigid plane

C. K. Lau and S. K. Tang[a)]
Department of Building Services Engineering, The Hong Kong Polytechnic University, Hong Kong, People's Republic of China

(Received 7 October 2004; revised 5 January 2006; accepted 12 January 2006)

The sound generated by a single vortex and by two identical vortices in the presence of a half-cylinder made of porous material mounted on a rigid horizontal plane is studied theoretically using the acoustic analogy and the matched asymptotic expansion method. Both longitudinal and transverse dipoles are observed upon the introduction of the porous cylinder, but the former is considerably stronger than the latter in all the cases studied. Results suggest that the amplitudes of the dipoles and the overall acoustical energy radiated can be higher than that in the rigid cylinder case under some suitable combinations of flow parameters, especially when the flow resistance inside the porous material seen by the vortices is very small. © *2006 Acoustical Society of America.* [DOI: 10.1121/1.2171838]

PACS number(s): 43.28.Ra, 43.50.Nm, 43.50.Gf [DRD] Pages: 2084–2095

I. INTRODUCTION

Noise is an unwanted byproduct from building services machinery, such as an air-conditioning unit, a fan coil unit, dampers, registers, louvers, guide vanes, etc. This noise propagates inside ventilation ducts conveying low Mach number turbulent flows and is usually attenuated by reactive or passive methods.[1] The most common device for this purpose is the dissipative silencer which dissipates sound energy by the viscous actions inside the porous material. Lighthill[2] established the importance of aerodynamic sound generation as a result of turbulence interaction, while Curle[3] extended the theory to include the influence of solid boundaries. Flow turbulence is expected to generate sound even in the presence of acoustically absorptive materials. The self-noise from a dissipative silencer is a typical example of such aerodynamic noise production.[4]

Theoretical studies usually deal with rigid wall boundaries,[5] and studies related to the characteristics of the porous materials on sound generation are rarely found in the existing literature. However, there are studies on the sound attenuation performance of a dissipative silencer in the absence of flow turbulence through different approaches. Examples include that of Cummings and Chang[6] who investigated the attenuation of a dissipative silencer of finite length with mean flow by mode matching technique, that of Quinn and Howe[7] who investigated theoretically the production and absorption of acoustic energy when a sound wave impinges on the edges of an acoustic lossless liner, and the finite element study of Peat and Rathi[8] on the sound fields inside dissipative silencers.

The results of Ffowcs Williams[9] show that sound is produced when flow turbulence is near sound-absorbent liners and thus provide further theoretical support to the self-noise production of dissipative silencers and acoustic wall linings. A recent study of the authors[10] deals with the vortex sound generation in the presence of a wedge made up partially of porous material. It is found that the additional acceleration of the vortex in the presence of the porous material has a significant effect on the radiated sound energy.[10]

Although vortices are a drastic simplification of real turbulence, they have provided insights into the generation processes of flow noises (for instance, Crighton).[11] In the present investigation, the sound generated by the unsteady motions of vortices in the proximity of a porous half-cylinder on an otherwise rigid horizontal plane is studied. The complex potential and the velocities of the vortices are evaluated through the use of conformal mapping as in Tang,[12] while the outer far-field potential is derived by using the matched asymptotic method as in Obermeier.[13] The present configuration is intended to represent one flow boundary inside a dissipative silencer. It is hoped that the present results can enhance the understanding of aerodynamic sound generation under the influence of porous surfaces and be useful in the future modeling of the self-noise generated by dissipative silencers.

II. THEORETICAL DEVELOPMENT

Two rectilinear vortices with circulations Γ_1 and Γ_2 initially located at the complex locations z_1 and z_2, respectively, interact with a half-cylinder composed of porous material as shown in Fig. 1(a). The height of each vortex above the rigid plane is denoted by h, while the horizontal vortex separation is represented by d. The properties of the porous material are characterized by the effective fluid density, ρ_e, and the flow resistance R_f inside its lattice.[14] The former represents the fluid inertia effect while the latter includes the effect of viscosity. Unless the fluid is perfectly inviscid, one should note that owing to the very tiny fluid passages inside the porous material, the effect of viscosity on the fluid motion inside

a)Author to whom correspondence should be addressed. Electronic mail: besktang@polyu.edu.hk

 0001-4966/2006/119(4)/2084/12/$22.50

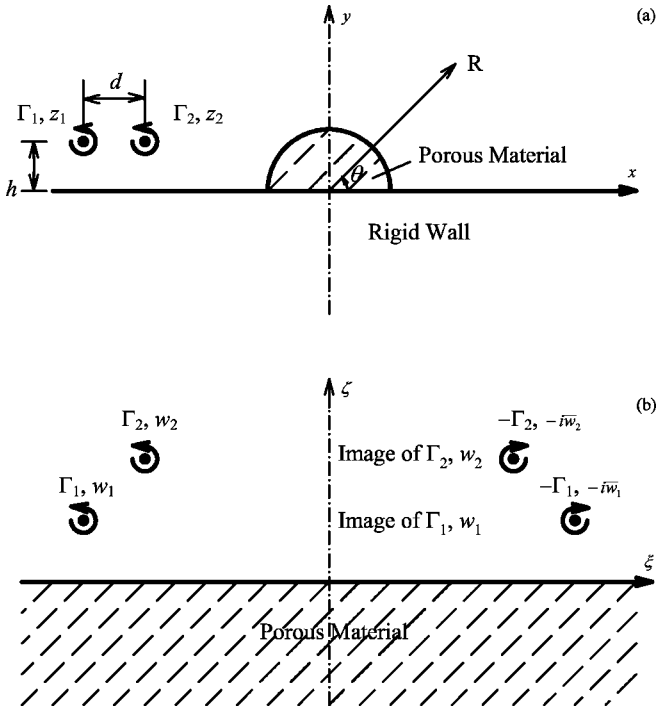

FIG. 1. Schematics of vortex model and nomenclatures: (a) Original z plane and (b) w plane.

this material cannot be neglected though the external flow outside it can be satisfactorily represented by the inviscid model.[12] Also, the introduction of the porous material results in finite surface flow impedance, which may lower the ability of this boundary to support fluid pressure and produce a pressure-releasing effect. More information on pressure-releasing boundaries can be found in, for instance, Schneider *et al.*[15]

The corresponding complex potentials and the velocities of the vortices can be worked out as in Tang and Lau.[10] With the help of the conformal mapping,[16] the original z-plane ($z=x+iy$) is transformed into the w-plane ($w=\xi+i\zeta$) as shown in Fig. 1(b), and the mapping function is

$$z = f(w) = -\frac{i+w}{i-w} \Rightarrow w = f^{-1}(z) = i\frac{z+1}{z-1}. \tag{1}$$

The stream function, Ψ_{wj}, and the transverse velocity, V_{wj}, of the jth vortex in the w plane can then be obtained by matching the fluid pressure and normal fluid velocity along the impedance boundary.[12] In the present study, all length scales are normalized by the cylinder radius a, and the strengths of the vortices are normalized by the total vortex strength Γ ($=\Gamma_1+\Gamma_2$). Here, time is normalized by a^2/Γ. V_{wj} and R_f are normalized by Γ/a and $\rho\Gamma/a^2$ respectively (ρ being the density of the incompressible fluid medium). The results of Tang[12] suggest that, for an isolated vortex j,

$$\Psi_{wj} = \frac{\Gamma_j}{4\pi}\int_{-\infty}^{\infty}\frac{1}{|k|}(e^{-|k|\zeta_j} + g_j e^{|k|\zeta_j})\frac{e^{-|k|\zeta}}{g_j}e^{ik(\xi_j-\xi)}dk, \tag{2}$$

where $g_j(k) = R_f + ikV_{wj}(1+m) \big/ -R_f + ikV_{wj}(1-m)$ and $m = \rho_e/\rho$. The corresponding vortex velocity is

$$V_{wj} = \frac{\Gamma_j}{4\pi}\int_{-\infty}^{\infty}\frac{-e^{-2|k|\zeta_j}}{g_j}dk. \tag{3}$$

The overall stream function, Ψ_w, in the presence of other vortices is therefore

$$\Psi_w = \sum_{j=1}^{4}\frac{\Gamma_j}{4\pi}\int_{-\infty}^{\infty}\frac{1}{|k|}(e^{-|k|\zeta_j} + g_j e^{|k|\zeta_j})\frac{e^{-|k|\zeta}}{g_j}e^{ik(\xi_j-\xi)}dk, \tag{4}$$

and the velocity of the jth vortex, u_{wj} and v_{wj}, in the w plane are

$$u_{wj} = V_{wj} + \sum_{l=1\neq j}^{4}\left.\frac{\partial\Psi_{wl}}{\partial\zeta}\right|_{\xi=\xi_j,\zeta=\zeta_j},$$

$$v_{wj} = -\sum_{l=1\neq j}^{4}\left.\frac{\partial\Psi_{wl}}{\partial\xi}\right|_{\xi=\xi_j,\zeta=\zeta_j}. \tag{5}$$

Also, $\Gamma_3=-\Gamma_1$, $u_{w3}=-u_{w1}$, $v_{w3}=v_{w1}$, and $\Gamma_4=-\Gamma_2$, $u_{w4}=-u_{w2}$, $v_{w4}=v_{w2}$. The paths of the vortices in the z plane are calculated by integrating Eq. (5) numerically using the standard fourth-order Runge–Kutta method together with the Routh's correction.[17]

It can be shown, as in Tang and Lau[10] with the Cauchy–Riemann principle, that

$$\phi_w = \sum_{j=1}^{4}\frac{1}{2\pi}\int_{0}^{\infty}\frac{\Gamma_j}{k}(e^{-k\zeta_j} + g_j e^{k\zeta_j})\frac{e^{-k\zeta}}{g_j}\sin(k(\xi_j-\xi))dk + C, \tag{6}$$

where C is the integration constant that can be evaluated by observing that the flow potential vanishes as $|z|\to\infty$. The incompressible flow potential in the z plane, ϕ_z, can then be found by substituting w by $f^{-1}(z)$ in Eq. (6). The far-field potential, ϕ_{zo}, can then be obtained using the matched asymptotic expansion.[13] The far-field sound pressure is

$$p = -\frac{\partial\phi_{zo}}{\partial t}, \tag{7}$$

where t is the far-field observer time and p is normalized by $\rho\Gamma^2/a^2$. The foregoing equations are specifically derived for the present study.

A. Perfectly inviscid fluid

When the flow resistance R_f inside the lattice of the cylinder vanishes, it can be shown using Ref. 18 that

$$g_j = \frac{1+m}{1-m}$$

and

$$C = -\sum_{j=1}^{4}\frac{\Gamma_j}{2\pi}\left(\frac{1}{g_j}\tan^{-1}\frac{\xi_j}{1+\zeta_j} + \tan^{-1}\frac{\xi_j}{1-\zeta_j}\right).$$

Morse and Ingard[14] remarked that $1<m<5$ for practical porous materials, but m can be very large if the porous material

is replaced by a hard solid. In the study of the transmission loss across dissipative silencers, the data in Peat and Rathi,[8] Cummings and Sormaz,[19] and Kirby[20] give $m \approx 2.5$. By substituting $w=f^{-1}(z)$ into Eq. (6), the flow potential in z plane is thus

$$\phi_z = \sum_{j=1}^{4} \frac{\Gamma_j}{2\pi} \mathrm{Im}\left\{ \frac{1}{g_j}\left[\ln\left(1-\frac{1}{z\bar{z}_j}\right) - \ln\left(1-\frac{1}{z}\right)\right] + \left[\ln\left(1-\frac{z_j}{z}\right) - \ln\left(1-\frac{1}{z}\right)\right]\right\}. \tag{8}$$

The far-field inner potential produced by the vortices in a perfectly inviscid fluid is, for large $|z|$,

$$\phi_{zi} = -\sum_{j=1}^{2} \frac{\Gamma_j}{\pi r}\left(r_j + \frac{1}{g_j r_j}\right)\sin(\theta_j)\cos\theta + O(r^{-2}), \tag{9}$$

where (r_j, θ_j) are the polar coordinates of the jth vortex and (r, θ) those of a point in the flow field.

The far field so produced in the frequency domain is the solution of the Helmholtz equation $\nabla^2\phi + k^2\phi = 0$, which is $\phi = \sum_{j=1}^{4} A_j H^{(1)}_{\alpha_j}(kr)e^{i\alpha_j\theta}$, where $H^{(1)}_{\alpha j}$ is the Hankel function of the first kind of order α_j, and k is the wave number. The matched asymptotic expansion[12] suggests that for low-frequency sound radiation, $\alpha_j = 1$ and $A_j = -\Gamma_j\omega/2c\left[\left(r_j + 1/g_j r_j\right)\sin(\theta_j)\right]^t$, where $k=\omega/c$, c is the ambient speed of sound and $[\ ]^t$ represent the Fourier transform with respect to time. At a large distance R, one obtains with the property of the Hankel function[21] that for positive ω,

$$\phi = -\sum_{j=1}^{2} \frac{\Gamma_j \omega}{2c}\left[\left(r_j + \frac{1}{g_j r_j}\right)\sin(\theta_j)\right]^t \sqrt{\frac{2c}{\pi\omega R}} e^{i(\omega R/c - 3\pi/4)}. \tag{10}$$

The far-field potential ϕ_{zo} can be obtained by using the inverse Fourier transform:

$$\phi_{zo} = -\frac{1}{2\pi}\sum_{j=1}^{2}\int_{-\infty}^{\infty} \frac{\omega\Gamma_j}{2c} \times \left[\left(r_j + \frac{1}{g_j r_j}\right)\sin(\theta_j)\right]^t \sqrt{\frac{2c}{\pi\omega R}} e^{i(\omega R/c - 3\pi/4)} e^{-i\omega t} d\omega. \tag{11}$$

Thus, the far-field sound pressure is

$$p = -\frac{\partial\phi_{zo}}{\partial t} = \frac{1}{\pi}\sqrt{\frac{1}{2c\mathrm{R}}}\sum_{j=1}^{2}\frac{\partial}{\partial t}\int_{-\infty}^{t-\mathrm{R}/c}\frac{\partial}{\partial\tau}\left[\left(r_j + \frac{1}{g_j r_j}\right)\sin(\theta_j)\right]\frac{\Gamma_j d\tau}{\sqrt{t-\tau-\mathrm{R}/c}}\cos\theta. \tag{12}$$

Equation (12) shows that the pressure generated in a perfectly inviscid fluid is a longitudinal dipole. For a rigid cylinder (very large m and $g_j \to -1$), it reproduces the result of Abou-Hussein *et al.*[22]

B. Combined effects of effective fluid density and flow resistance

When the flow resistance R_f is finite, the effects from the porous material become complicated. The flow potential in the w plane is

$$\phi_w = \sum_{j=1}^{4}\frac{\Gamma_j}{2\pi}\left\{ -\tan^{-1}\frac{\xi_j-\xi}{\zeta+\zeta_j} + \tan^{-1}\frac{\xi_j-\xi}{\zeta-\zeta_j} + \frac{2}{1+m}\int_0^\infty \frac{k e^{-k(\zeta+\zeta_j)}\sin(k(\xi_j-\xi))}{(\beta_j^2+k^2)}dk + \frac{2R_f}{|V_{wj}|(1+m)^2}\int_0^\infty \frac{e^{-k(\zeta+\zeta_j)}\cos(k(\xi_j-\xi))}{\beta_j^2+k^2}dk + C\right\}, \tag{13}$$

where

$$C = \sum_{j=1}^{4}\frac{i\Gamma_j}{2\pi}\left\{ -\mathrm{Re}[\ln(1+i\bar{w}_j)] + \mathrm{Re}[\ln(1+iw_j)] - \frac{2}{1+m}\mathrm{Im}[-ci(\beta_j\mu_j)\cos(\beta_j\mu_j) - si(\beta_j\mu_j)\sin(\beta_j\mu_j)] - \frac{2}{1+m}\mathrm{Re}[ci(\beta_j\mu_j)\sin(\beta_j\mu_j) - si(\beta_j\mu_j)\cos(\beta_j\mu_j)]\right\},$$

where $\bar{w}_j$=conjugate of w_j, $\mu_j = (1+\zeta_j) - i\xi_j$ and $\beta_j = R_f/[|V_{wj}|(1+m)]$, and *si* and *ci* are the sine and cosine integrals, respectively. The velocity of each vortex has to be estimated by iteration as in Tang and Lau[10] and Tang.[12]

The corresponding flow potential ϕ_z is

$$\phi_z = \sum_{j=1}^{4}\frac{\Gamma_j}{2\pi}\left[-\mathrm{Im}\left\{\ln\left(1-\frac{1}{z\bar{z}_j}\right) - \ln\left(1-\frac{z_j}{z}\right)\right\} + \frac{2}{1+m}\mathrm{Im}\left\{\begin{array}{l}[-ci(\beta_j\eta_j)\cos(\beta_j\eta_j) - si(\beta_j\eta_j)\sin(\beta_j\eta_j)] \\ -[-ci(\beta_j\mu_j)\cos(\beta_j\mu_j) - si(\beta_j\mu_j)\sin(\beta_j\mu_j)]\end{array}\right\} + \frac{2}{1+m}\mathrm{Re}\left\{\begin{array}{l}[ci(\beta_j\eta_j)\sin(\beta_j\eta_j) - si(\beta_j\eta_j)\cos(\beta_j\eta_j)] \\ -[ci(\beta_j\mu_j)\sin(\beta_j\mu_j) - si(\beta_j\mu_j)\cos(\beta_j\mu_j)]\end{array}\right\}\right], \tag{14}$$

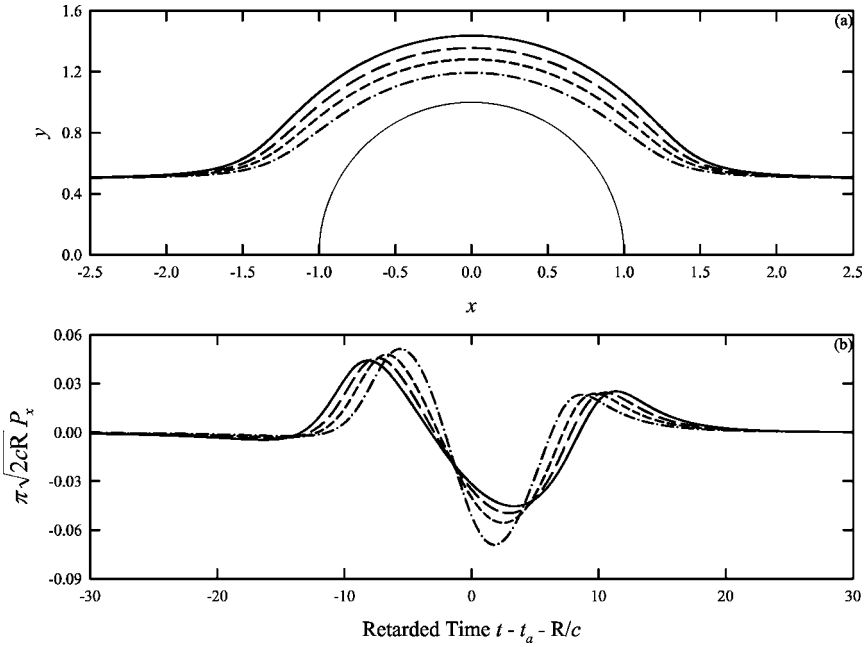

FIG. 2. Effect of pressure-releasing surface on vortex motion and sound generation: (a) Vortex path and (b) sound pressure. Initial $z_1=(-10,0.5)$. $-\cdot-$: $m=3$; - - -: $m=5$; — — —: $m=10$; and ——: Rigid cylinder.

where $\eta_j=(\zeta+\zeta_j)-i(\xi_j-\xi)$. The flow potential ϕ_{zi} at large $|z|$ becomes

$$\phi_{zi}=\sum_{j=1}^{4}\frac{\Gamma_j}{2\pi r}\left[\left(r_j-\frac{1}{r_j}\right)\sin(\theta-\theta_j)-f_{1j}\cos\theta - f_{2j}\sin\theta\right], \tag{15}$$

where

$$f_{1j}=\frac{2\beta_j}{1+m}\,\mathrm{Re}[\exp(i\gamma_j\beta_j)G(0,i\gamma_j\beta_j)+\exp(-i\gamma_j\beta_j)G(0,-i\gamma_j\beta_j)],$$

$$f_{2j}=\frac{4\beta_j}{1+m}\,\mathrm{Im}[ci(\gamma_j\beta_j)\cos(\gamma_j\beta_j)+si(\gamma_j\beta_j)\sin(\gamma_j\beta_j)],$$

$\gamma_j=1+r_je^{i\theta_j}+1/r_je^{i\theta_j}-1$, and $G(0,\chi)$ is the incomplete gamma function.[21] The far-field outer potential, ϕ_{zo}, can be obtained in the same way as in the previous two cases. Equation (15) indicates that a transverse dipole of magnitude f_{2j} exists when the flow resistance is finite. A longitudinal dipole of magnitude f_{1j} adds to the cylinder dipole. These findings have not been reported elsewhere.

One should also note that R_f in the present study is normalized by $\rho\Gamma/a^2$. Therefore, this parameter can vary over a very wide range. For weak vortex strength, R_f can be very large and it decreases as the vortex strength increases. It vanishes in the case of a perfectly inviscid fluid. The parameter ranges for real/experimental flows[19,20,23–27] are summarized in the Appendix for the sake of comparison with those in the present study. One can notice from the later discussions that the acoustic radiation with $R_f=100$ is already close to those of the rigid cylinder. In the foregoing discussions, the far-field sound pressure is evaluated at a radial distance R of 100.

III. RESULTS AND DISCUSSIONS

A. Single vortex

The paths of a single vortex translating over a rigid wall mounted half-cylinder and the corresponding sound radiations under different speeds of the mean flow have been studied by Abou-Hussein *et al.*[22] The magnitude of the sound pressure increases as h decreases. Active sound generation is observed during the period when the vortex undergoes a substantial rate of change of velocity when it is close to the cylinder. A single vortex moving over a rigid plane generates no sound.

For a perfectly inviscid fluid, the flow resistance vanishes ($R_f=0$). Figure 2(a) shows the effect of m on the vortex path with initial $h=0.5$. The path of a single vortex engaging a rigid wall mounted half-cylinder is also shown for comparison. The present theory indicates that the vortex path converges to that for the rigid wall condition at very large m. The vortex path bends toward the cylinder surface because of the pressure-releasing effect. The smaller the value of m, the greater the degree of bending toward the cylinder surface. This is similar to the case where a vortex moves in the vicinity of a wedge with inhomogeneous surface flow impedance.[12] The vortex resumes its original height as it gradually moves away from the cylinder (at $x>2$). When the initial h increases, less severe vortex path bending can be observed at a fixed m.

Equation (12) suggests that the far-field sound pressure is a longitudinal dipole (P_x) for a hard cylinder ($g_j\to-1$) or a perfectly inviscid fluid ($g_j=(1+m)/(1-m)$). The sound pressure increases [Fig. 2(b)] as the vortex comes closer to the cylinder surface and undergoes substantial longitudinal and transverse accelerations. The time t_a hereinafter, unless otherwise specified, denotes the time at which the vortex passes across the y axis ($x=0$). The pressure fluctuation patterns for various m are pulselike and are similar to that in the

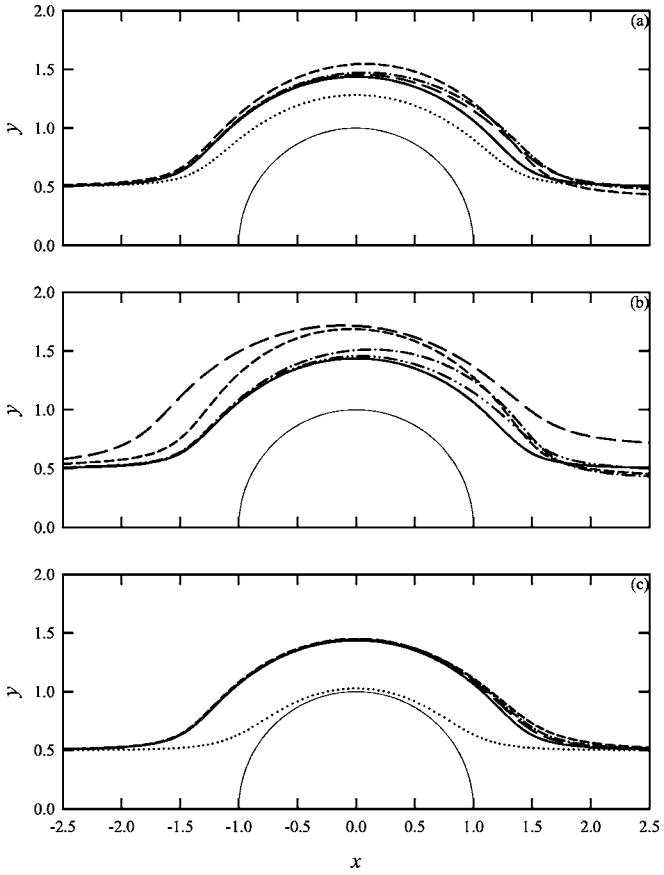

FIG. 3. Combined effects of effective fluid density and flow resistance on the vortex path. (a) $m=5$; ·····: $R_f=0$; - - -: $R_f=1$; −·−: $R_f=5$; — — —: $R_f=10$; and ——: Rigid cylinder. (b) $R_f=5$; −·−·−: $m=3$; −·−: $m=10$; - - -: $m=100$; — — —: $m=1000$; and ——: Rigid cylinder. (c) $m=1.5$. ·····: $R_f=0$; - - -: $R_f=1$; −·−: $R_f=5$; — — —: $R_f=10$; and ——: Rigid cylinder. Initial location of the vortex at $x=-10$ with initial $h=0.5$.

case of a hard cylinder, except that the duration of active sound production is reduced as m decreases. Amplifications of the first peak and trough of the pressure fluctuations are observed after the introduction of the porous material. The extent of such amplification increases with decreasing m. It is found that a decrease in either the initial h or m will lead to an increase in the strength of the far-field sound pressure fluctuation.

For a finite flow resistance ($R_f \neq 0$), previous results suggest that m and R_f produce reactive and resistive effects respectively.[12,14] Figure 3(a) shows such effects on the vortex path at a fixed m with the vortex initially located at $x=-10$ with $h=0.5$. The vortex paths for $R_f > 10$ are close to that of the rigid cylinder case and thus are not presented. The vortex moves away from the cylinder surface at $x<2$ for $1 \leqslant R_f < 10$. Further away from the cylinder at $x>2$, it is observed that the vortex height decreases when R_f is increased from 0 to 1, but it gradually rises back to $y=0.5$ at larger R_f. It is expected that when R_f is reduced toward zero, the pressure-releasing effect becomes more important such that the vortex path bends toward to the cylinder again and converges to that of the perfectly inviscid fluid case. One can also notice from Fig. 3(a) that the vortex paths under a finite R_f are not symmetrical about the y axis.

Figure 3(b) illustrates the effects of m on the vortex path with R_f fixed at 5. The vortex path bends away from the cylinder surface as in Fig. 3(a). The degree of the initial path bending increases with m for $m \leqslant 1000$. The vortex height h after the vortex passes over the cylinder first drops below 0.5 as m increases from 3, but rises up above 0.5 as m further increases from 10. One is expecting that h will resume the value of 0.5 as $m \to \infty$. When m is close to unity, the pressure-releasing effect is very strong. The vortex comes very close to the cylinder surface if the fluid is perfectly inviscid, but its path approaches that under the hard wall condition as R_f is increased as shown in Fig. 3(c).

Unlike the situation in an inviscid flow, the present far-field sound pressure consists of a longitudinal dipole, P_x, and a transverse dipole, P_y [Eq. (15)]. Figures 4(a) and 4(b) show some examples of the time variations of P_x and P_y for $m=5$ at various R_f, respectively. It is observed that the intro-

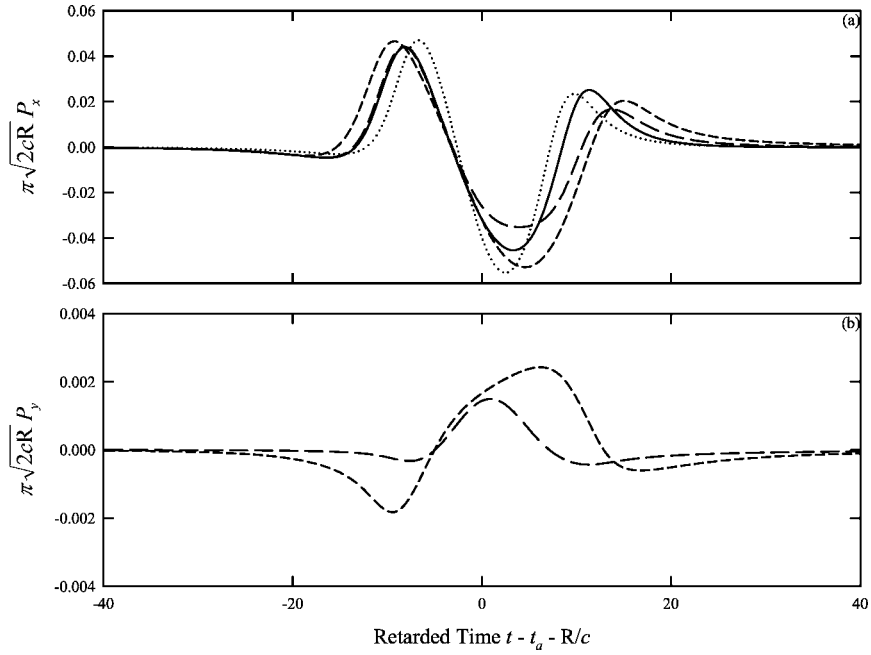

FIG. 4. Sound pressure time variation for $m=5$ at different R_f: (a) Longitudinal dipole and (b) transverse dipole. ·····: $R_f=0$; - - - -: $R_f=1$; — — —: $R_f=10$; and ——: Rigid cylinder.

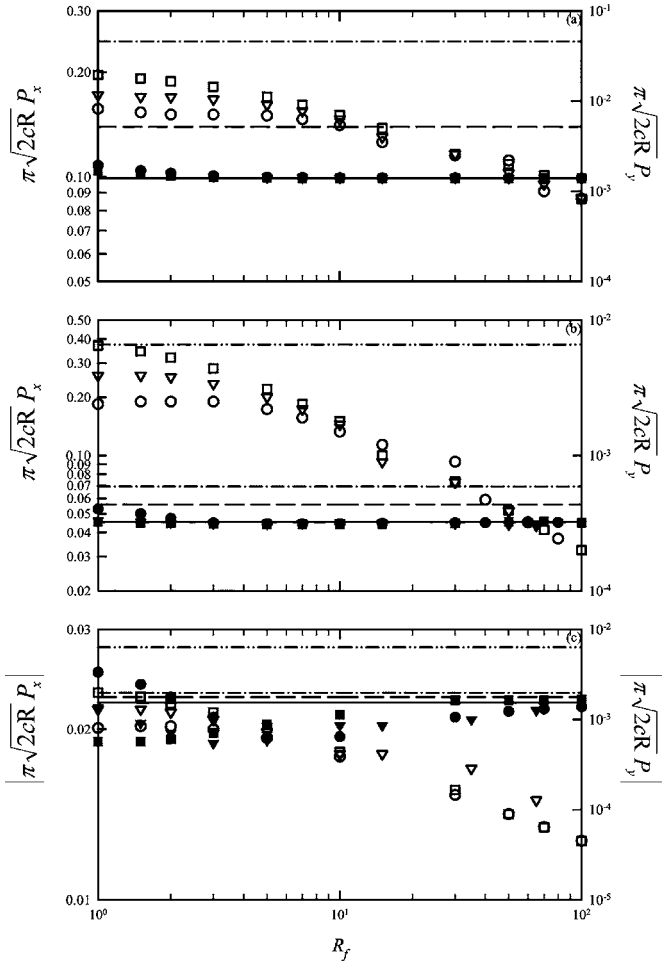

FIG. 5. Combined effects of effective fluid density, flow resistance, and initial vortex height on radiated sound amplitude: (a) $h=0.3$; (b) $h=0.5$; and (c) $h=0.8$. $-\cdot\cdot-$: P_x for $m=1.5$, $R_f=0$; $-\cdot-$: P_x for $m=3$, $R_f=0$; — — —: P_x for $m=5$, $R_f=0$; and ——: Rigid cylinder. □: $m=1.5$; ▽: $m=3$; and ○: $m=5$. Closed symbols for P_x; open symbols for P_y.

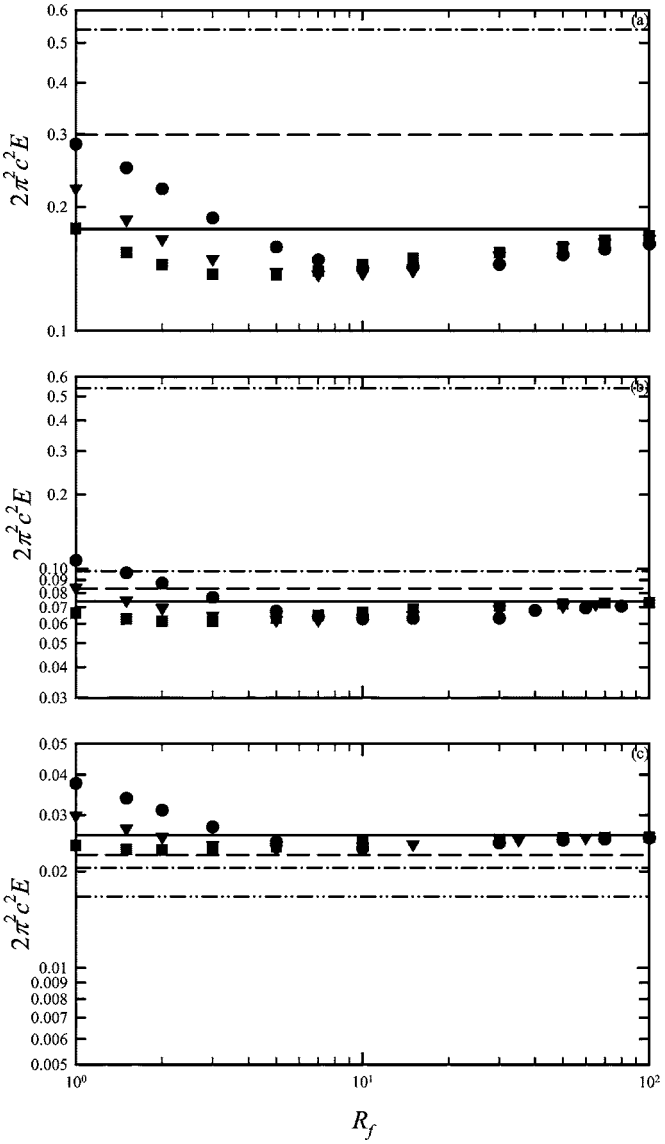

FIG. 6. Combined effects of effective fluid density, flow resistance, and initial vortex height on acoustical energy radiation: (a) $h=0.3$; (b) $h=0.5$; and (c) $h=0.8$. $-\cdot\cdot-$: P_x for $m=1.5$, $R_f=0$; $-\cdot-$: P_x for $m=3$, $R_f=0$; — — —: P_x for $m=5$, $R_f=0$; and ——: Rigid cylinder. ■: $m=1.5$; ▼: $m=3$; and •: $m=5$.

duction of a finite R_f has prolonged the duration of active sound radiation and has also resulted in the earlier radiation of sound. However, the magnitude of P_x is higher than the rigid cylinder condition for small R_f. The time variation of P_x converges to those for the rigid cylinder and perfectly inviscid fluid cases as $R_f\to\infty$ and 0, respectively. On the other hand, the introduction of the flow resistance enhances the radiation of P_y, though their magnitudes are small compared to those of P_x. The duration of the transverse dipole radiation appears longer than those of the longitudinal one. In addition, the magnitude of P_y is higher at some finite R_f. At very large R_f, the results converge to those in the rigid half-cylinder case.

Figures 5(a) to 5(c) summarize the effects of m and R_f on the amplitudes of P_x and P_y at $h=0.3$, 0.5, and 0.8 respectively for $1\leqslant R_f\leqslant 100$. The P_x for the cases of a rigid cylinder and an inviscid fluid are included for the sake of easy referencing. At an initial $h=0.3$, the amplitude of P_x is approximately equal to that of the rigid cylinder case for $R_f>1$ for all m studied [Fig. 5(a)]. The amplitude of P_y decreases as R_f is increased from 1 toward ∞ (for $R_f\to 0$ and ∞, $P_y=0$). The decrease of m increases the amplitudes of P_y for the whole range of R_f presented.

The increase of m leads to a reduction of the transverse dipole amplitude for the other two values of initial h for $R_f\geqslant 30$ [Figs. 5(b) and 5(c)]. The magnitude of the transverse dipole becomes weaker when the cylinder is less pressure releasing as anticipated by the theory (larger m and/or higher R_f). As can be expected, the increase in the initial vortex height h reduces the effects of the cylinder on the sound radiation. The results shown in Fig. 5 suggest that certain combinations of m and R_f will lead to louder sound radiation than the rigid cylinder case. Also, it is noted that the amplitudes of P_y are always below those of P_x, but the difference decreases with increasing initial h.

Figure 6 illustrates the overall acoustical energy (E) radiated by the unsteady vortex motions under the influence of m and R_f. At small initial h [Fig. 6(a)], the introduction of the porous material enhances the radiation of acoustical energy at $m=5$ and small R_f. This radiation becomes less important

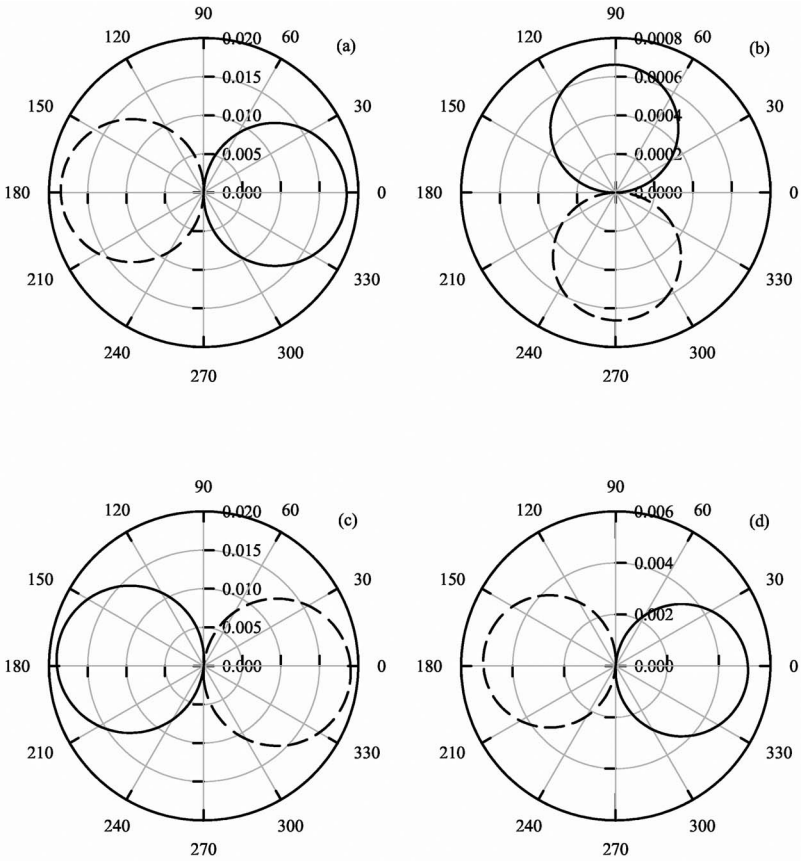

FIG. 7. Time variation of far-field directivity: (a) $t-t_a-\mathrm{R}/c=-13.55$; (b) $t-t_a-\mathrm{R}/c=-5.55$; (c) $t-t_a-\mathrm{R}/c=4.46$; and (d) $t-t_a-\mathrm{R}/c=24.89$. Initial $z_1=(-10,0.8)$, $m=1.5$ and $R_f=1.5$. — — —: negative sound pressure; ——: positive sound pressure.

as m decreases from 5 to 1.5. As R_f is increased, the strength of the energy radiation eventually falls below that in the rigid cylinder case for a fixed m. However, all the curves in Fig. 6(a) converge to $E=0.1769$, which is the energy radiated in the rigid cylinder case, for large R_f.

The situations at initial $h=0.5$, presented in Fig. 6(b), follow closely those shown in Fig. 6(a). The increase in the initial h reduces the induction effect of the cylinder, resulting in less significant sound radiation even at small m and R_f. Further increase in the initial h to 0.8 does not affect much the trend of E variation with R_f and m for $R_f>1$ [Fig. 6(c)]. In this case, less acoustical energy than in the rigid cylinder case is radiated at $R_f\rightarrow 0$ for all m.

Figures 7(a) to 7(d) show the change in the directivity patterns of the sound radiation. One can notice that the dipole axis does change with time as in Minota and Kambe,[28]

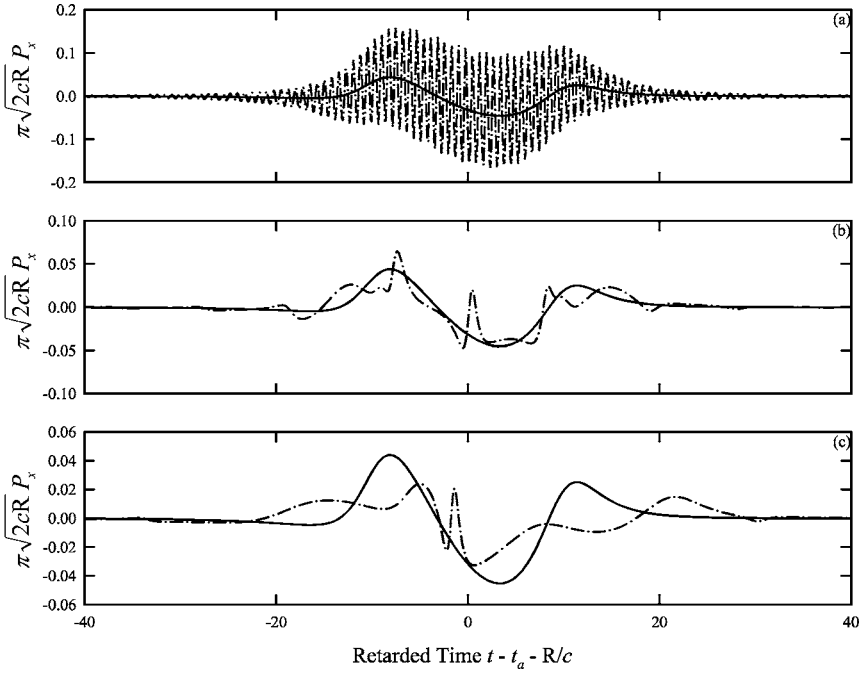

FIG. 9. Time variation of longitudinal dipole magnitude at different separation distance in the presence of a rigid cylinder: (a) $d=0.2$; (b) $d=0.8$; and (c) $d=1.6$. ——: Equivalent single vortex results; and $-\cdot-$: Two interacting identical vortices results. z_c initially at $(-10,0.5)$, $\Gamma_1=\Gamma_2=0.5$.

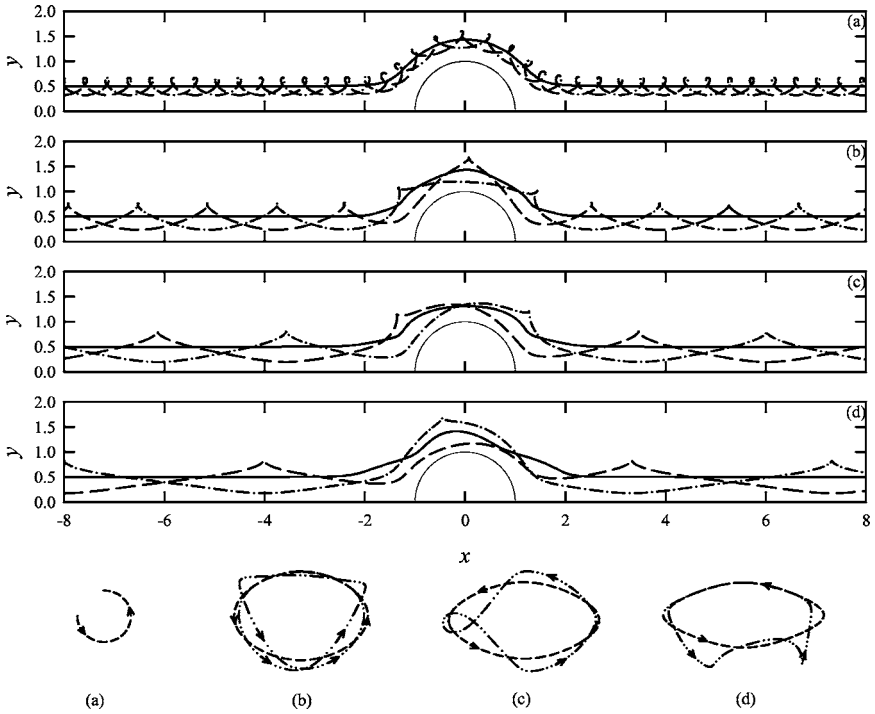

FIG. 8. Unsteady leapfrogging motions of two identical vortices near a rigid cylinder: (a) $d=0.4$; (b) $d=0.8$; (c) $d=1.2$; and (d) $d=1.6$. Initial $z_c=(-10,0.5)$, $\Gamma_1=\Gamma_2=0.5$. — — —: z_1; $-\cdot-$: z_2; ——: z_c; - - - -: z_1 relative to z_c at $x<-2$ or $x>2$; and $-\cdots-$: z_2 relative to z_c at $-2<x<2$.

but it should be noted that the longitudinal dipole dominates the sound field as the magnitude of P_x is nearly always higher than that of P_y (Fig. 5). The rotation of the dipole axis can only be observed when P_x is sufficiently small, which is also the instant of less significant sound radiation.

B. Two interacting identical vortices

The sound generation by two identical vortices will be examined in this section. The initial vertical height of the vortices h is set at 0.5 and the strengths of the two vortices are set equal at $\Gamma_1=\Gamma_2=0.5$. It is well known that two vortices of thin cores will undergo leapfrogging and such motion is periodic in the absence of the cylinder.[29] A quadrupole field is also created but its magnitude is too small when compared to the dipole fields in the present low Mach number vortex motion and thus is ignored. In the foregoing discussions, the vorticity centroid of the two vortices is defined as $z_c=(\Gamma_1 z_1+\Gamma_2 z_2)/\Gamma$, where $\Gamma=\Gamma_1+\Gamma_2$. Similar to the previous section, the results associated with the combinations of m and R_f under which the vortices come very close to the cylinder surface are excluded from the presentation.

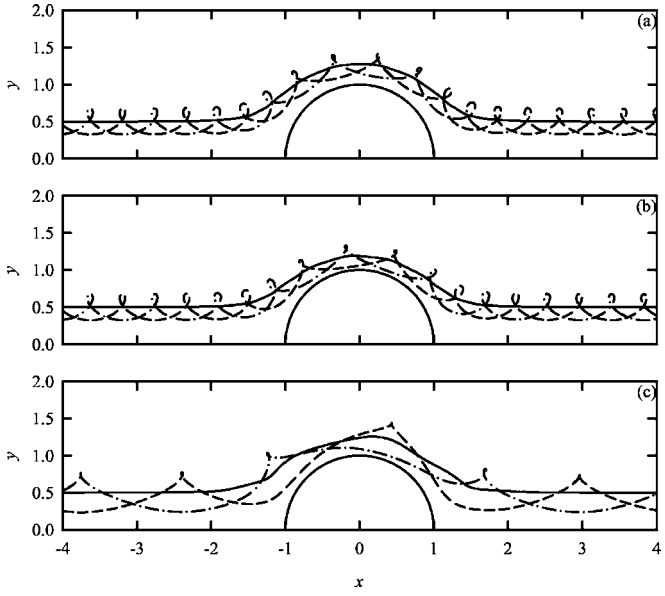

FIG. 10. Paths of two interacting vortices for perfectly inviscid fluid cases: (a) $d=0.4$, $m=5$; (b) $d=0.4$, $m=2$; and (c) $d=0.8$, $m=5$. z_c initially at $(-10,0.5)$, $\Gamma_1=\Gamma_2=0.5$. — — —: z_1; $-\cdot-$: z_2; and ——: z_c.

Figure 8 illustrates some examples of the vortex paths at different d in the presence of a rigid cylinder. The paths of the individual vortices relative to z_c are also given at the bottom of the figure. For $d\leqslant 0.4$, the path of the vorticity centroid collapses with that of a single vortex of strength $\Gamma=1$ initially located at $x=-10$ with $h=0.5$. The paths of the vortices are circular relative to the vorticity centroid [Fig. 8(a)]. The presence of the cylinder does not much affect the mutual induction between the two vortices within this range of d.

At increased d, the path of z_c deviates from that shown in Fig. 8(a), and the paths of the two vortices relative to the vorticity centroid become chaotic and noncircular. The leapfrogging vortex motions become more disturbed as d increases from 0.8 to 1.6 [Figs. 8(b) to 8(d)]. The larger vortex separation weakens the mutual induction strengths between the vortices.

Figures 9(a) to 9(c) show the far-field sound pressure time fluctuations at different d. It is expected that the sound radiation is more significant when the vortices are in the proximity of the cylinder. The periodic leapfrogging vortex motions at small d result in a faster time fluctuating sound pressure [Fig. 9(a)], which carries most of the sound energy. There is a slowly varying component embedded inside the result shown in Fig. 9(a), which is similar to that produced by a single vortex of strength $\Gamma=1$ initially located at z_c

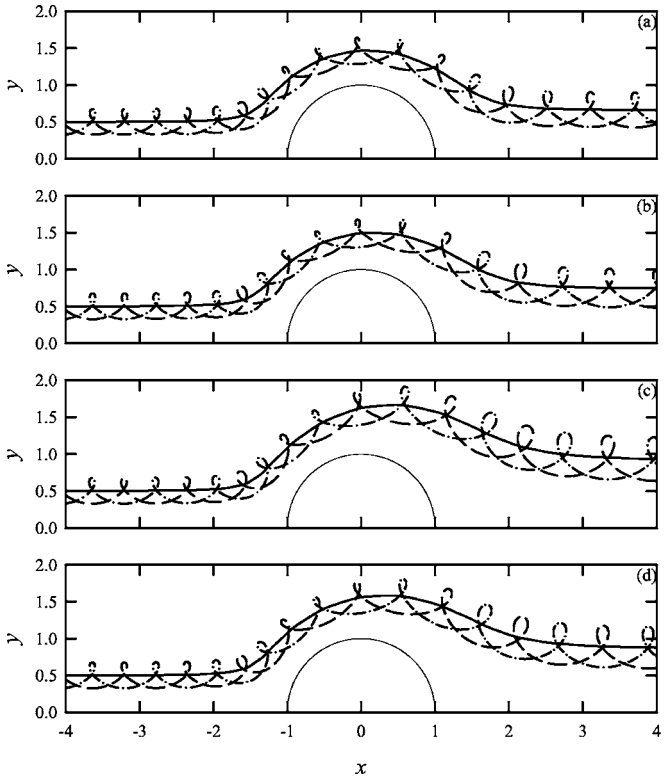

FIG. 11. Combined effects of effective fluid density and flow resistance on the vortex paths: (a) $m=5$, $R_f=10$; (b) $m=5$, $R_f=5$; (c) $m=5$, $R_f=1$; and (d) $m=3$, $R_f=1$. Initial $z_1=(-10.2,0.5)$, initial $z_2=(-9.8,0.5)$, $\Gamma_1=\Gamma_2=0.5$, $d=0.4$. — — —: z_1; –·–: z_2; and ——: z_c.

$=(-10,0.5)$. The increase in d leads to less ordered leapfrogging vortex motions. The pulses in Figs. 9(b) and 9(c) are created at the instant the vortex slip-through occurs as in the case without the cylinder.[30]

As discussed in Fig. 2(a), a finite effective fluid density inside the porous material lattice will create a pressure-releasing effect, reducing the effects of the cylinder relative to the mutual induction between the vortices. At $d=0.4$, ordered periodic vortex leapfrogging can be observed when $m=5$ and $R_f=0$ [Fig. 10(a)]. The reduction of m to 3 does not disturb much the leapfrogging vortex motions though the vortex paths are much closer to the cylinder surface [Fig. 10(b)]. The same is also true for $m=2$ (not shown here). The stronger effect from the cylinder due to shorter separation between it and the vortices does result in a slight deviation of the vortex paths relative to z_c from circular motion. The path of z_c resembles those shown in Fig. 2(a). Similar observations can be made at increased d [for instance, Fig. 10(c)] provided that the vortices do not hit the cylinder.

When the flow resistance inside the cylinder is finite, the vortex paths tend to bend away from the cylinder surface as the vortices propagate across the cylinder (Fig. 11) as in the single vortex case (Fig. 3). However, unlike the cases with a rigid cylinder or a perfectly inviscid fluid [Figs. 8 and 10, respectively], an increase in the pairing period is observed in the present two interacting vortices case upon the introduction of R_f. The separation of the vortices eventually increases due to the combined effect of m and R_f (Fig. 11). Decreasing m at a fixed R_f (for $R_f \geqslant 1$) brings the vortices closer to the x-axis after they pass over the cylinder into the region $x>2$ [Figs. 11(c) and 11(d)] and increases the frequency of the sound radiated. Such increase in sound frequency is more pronounced at small d. However, one should note that the acoustical energy radiated when the vortices are at $|x|>2$ is much less important. The dynamic at increased d is similar to those presented in Fig. 11, though one expects the two vortices will move closer to the cylinder provided that no impingement occurs. Thus, they are not presented.

Figures 12(a) and 12(b) illustrate the time variations of P_x and P_y at different R_f, respectively, at $d=0.4$ and $m=5$. Here, t_a represents the instant when the vorticity centroid passes over $x=0$. One can observe that there are fast and slow time varying components in P_x [Fig. 12(a)]. The former is due to the nominally circular motion of the vortices relative to z_c, whose frequency decreases after the vortices pass

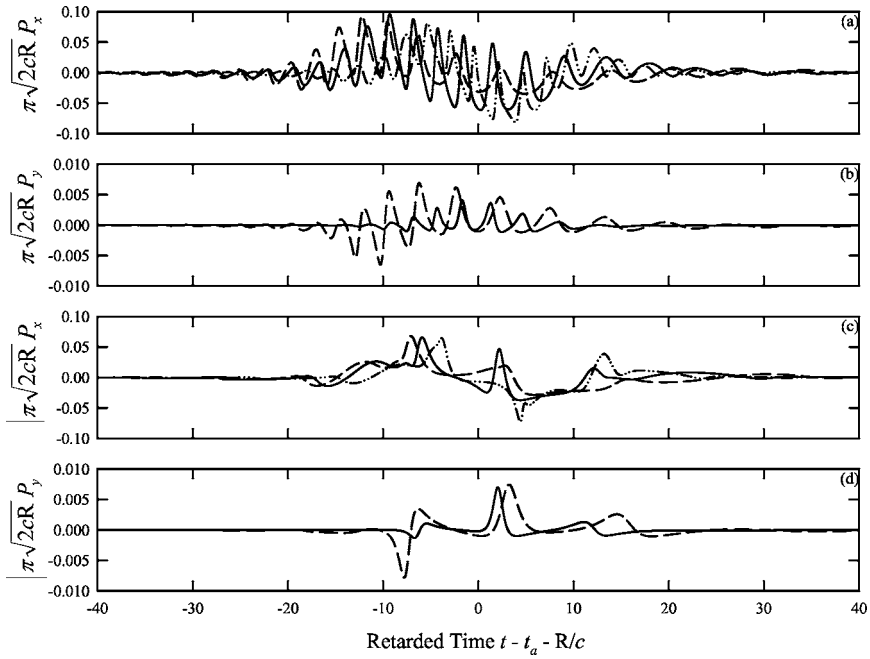

FIG. 12. Examples of time variation of dipole magnitudes at finite effective fluid density and flow resistance: (a) P_x, $d=0.4$; (b) P_y, $d=0.4$; (c) P_x, $d=0.8$; and (d) P_y, $d=0.8$. –···–: $R_f=0$; — — —: $R_f=1$; and ——: $R_f=10$. Initial $z_c=(-10,0.5)$, $\Gamma_1=\Gamma_2=0.5$.

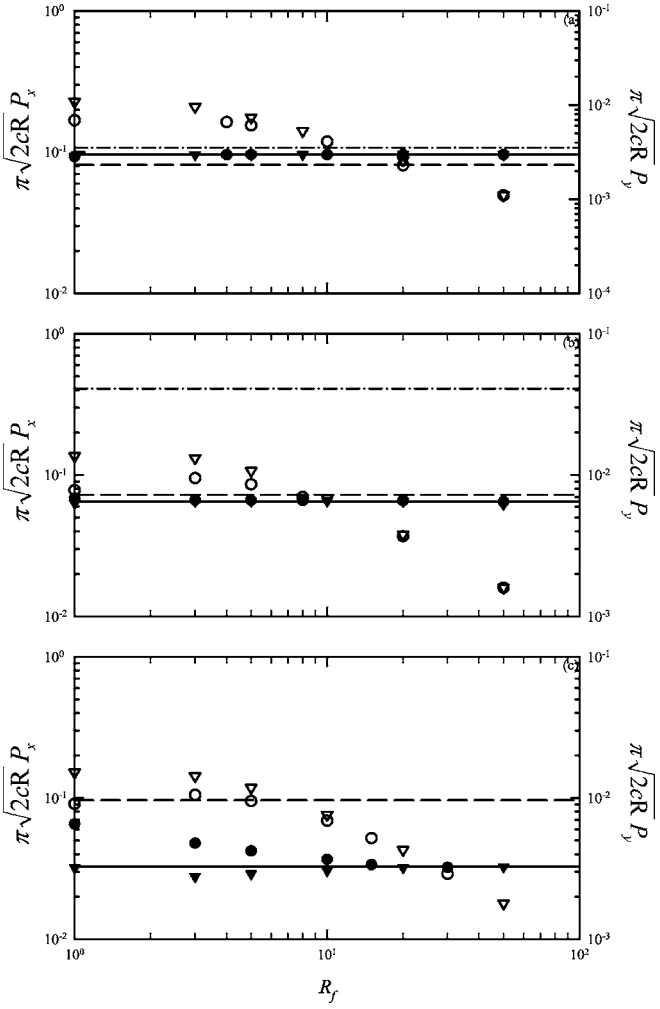

FIG. 13. Amplitudes of the dipoles produced by two interacting identical vortices: (a) $d=0.4$; (b) $d=0.8$; and (c) $d=1.6$. Initial $z_c=(-10,0.5)$, $\Gamma_1=\Gamma_2=0.5$. Legends: Same as those in Fig. 5.

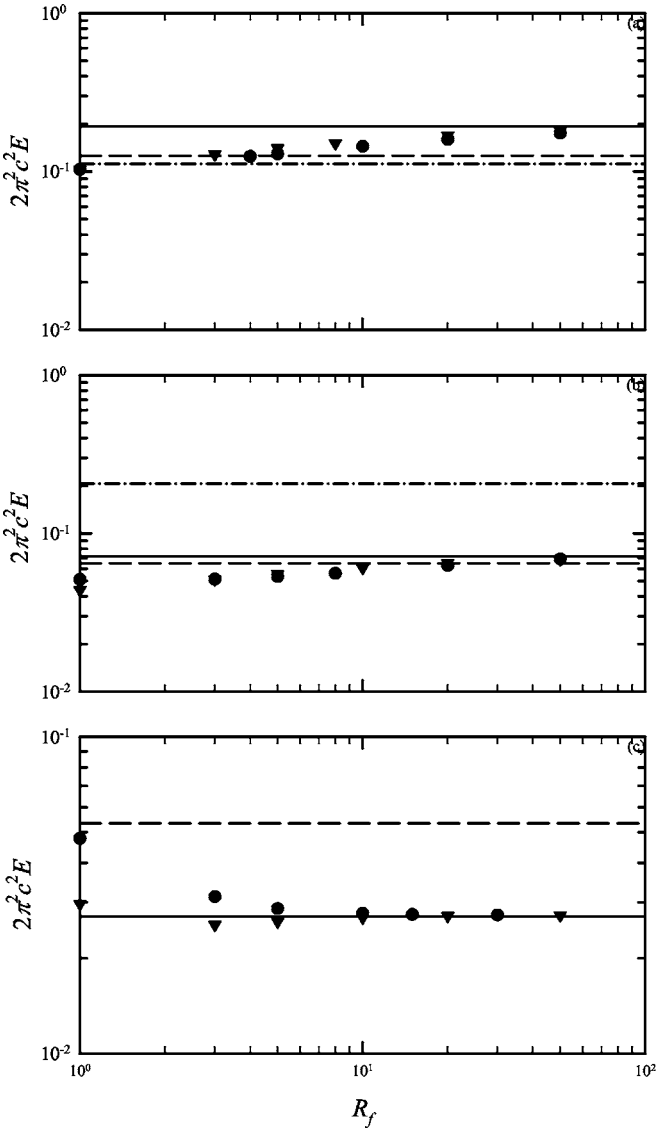

FIG. 14. Acoustical energy radiated by two interacting identical vortices: (a) $d=0.4$; (b) $d=0.8$; and (c) $d=1.6$. Initial $z_c=(-10,0.5)$, $\Gamma_1=\Gamma_2=0.5$. Legends: Same as those in Fig. 6.

over the cylinder. The strength of this component relative to the slow time varying one increases with increasing R_f for $R_f>1$. Similar time varying components are also found in P_y [Fig. 12(b)], but the amplitudes are very small when compared to those found in P_x. The amplitudes of these time varying components first increases with R_f but they decrease as R_f increases beyond unity. P_y vanishes when $R_f=0$ or $R_f\rightarrow\infty$.

The increase in the separation d to 0.8 reduces the mutual induction strength between the vortices, resulting in much less regular leapfrogging motions. The corresponding time variations of P_x and P_y with finite R_f are given in Figs. 12(c) and 12(d), respectively. The results for the hard cylinder at $d=0.8$ have been shown in Fig. 9(b). One can notice that the amplitudes of the two dipoles for $d=0.4$ and 0.8 do not differ much, but the higher-frequency fluctuations at $d=0.4$ imply more significant radiation of acoustical energy.

Figure 13 illustrates the dependence of the amplitudes of P_x and P_y on R_f, m and d. Again the amplitude of P_y is about a half- or a full-order below that of P_x. It is found that the introduction of the porous cylinder reduces in general the amplitude of the longitudinal dipole P_x for small d for $m\geqslant 3$ [Fig. 13(a)]. The vortices can be very close to the cylinder or even hit the cylinder when m drops below 3, making the whole vortex approach invalid, and the corresponding results are not presented.

The increase in d appears to have amplified P_x above its corresponding magnitude in rigid cylinder situation for $m=5$ [Figs. 13(b) and 13(c)]. The trend of P_x variation with d shown in Fig. 13 suggests louder noise will occur upon an increase of d. This implies that the presence of a porous material near a jet shear layer can be noisier than the case where the porous material is replaced by a rigid one, if the material is not located at a position where the dominant flow structures have a short wavelength (the initial shear layer mode).[31] Figure 14 further suggests that the porous material can reduce the overall acoustical energy radiation when d is small. It can also be noted that E decreases with decreasing m. The sound produced by the mutual interaction of the vortices depends very much on the unsteady leapfrogging motions. The smaller the value of d, the higher the frequency of the radiated sound, and thus weaker sound radiation can be

TABLE I. Ranges of parameters in practical and experimental flows.

Parameter	Typical range	Normalized range
Cylinder radius (cm)[a]	10–15	1
Vortex spacing (cm)[b]	0.6–10.2	0.04–1.02
Vortex height (cm)[c]	0–6.7	0–0.67
Flow speed (m/s)	0–40	0–43
Vortex circulation (m^2/s)[d]	0.14–3.4	1
Effective fluid density[e]	1–3	1–3
Flow resistance (kg/m^3s)[e,f]	2000–75 000	4.9–10 000

[a]See Ref. 24.
[b]See Ref. 25.
[c]See Refs. 34–36.
[d]See Refs. 26 and 33.
[e]See Refs. 19, 20, and 23.
[f]See Ref. 27.

expected because of the sound absorption property of the porous material. The effects of initial h in this two interacting vortices case are similar to those observed in the single vortex case and thus are not discussed further.

An external mean flow is absent in the present study. However, its presence is not expected to alter the sound generation process. On the contrary, the mean flow will result in a vortex path closer to the cylinder and the associated higher rate of change of vortex velocity will probably create a stronger sound field. The convective amplification of sound as in the case of Ffowcs Williams and Lovely[32] is also anticipated. The present results therefore represent the weakest sound radiation of the topic.

IV. REMARKS

The low Mach number condition in the present study results in the radiation of low frequency sound whose peak value depends substantially on the vortex circulation. At $R=100$ with an ambient speed of sound $c=343$ (normalized by Γ/a), $h=0.3$ and $m=1.5$, the maximum peak normalized sound pressure radiated at $R_f=1$ by a single vortex is 1.3×10^{-4} [Fig. 5(a)]. With a $\Gamma=0.14$ m^2/s, the maximum sound pressure level is around 23.5 dB, but this pressure level goes up to ~78.9 dB when $\Gamma=3.4$ m^2/s. For a rigid half-cylinder, the corresponding maximum sound pressure levels are 21 dB and 72 dB, respectively.

In the case of two vortices with $h=0.5$, $d=0.8$, $m=5$, and $R_f=1$, the sound pressure levels with $\Gamma=0.14$ m^2/s and 3.4 m^2/s are approximately 19.8 dB and 75.2 dB, respectively [Fig. 13(b)]. The corresponding values for rigid half cylinder are 19.3 dB and 74.7 dB, respectively.

The above dimensional examples illustrate that the aeroacoustics studied in the present work can be significant, and the introduction of porous material can enhance the sound radiation at certain combinations of parameters.

V. CONCLUSIONS

In the present investigation, the sound generation by the unsteady motions of vortices in the presence of a porous half cylinder on an otherwise rigid horizontal plane is studied theoretically. The far-field sound pressure so produced is evaluated through the use of conformal mapping and matched asymptotic method. The effects of the effective fluid density and flow resistance inside the porous materials on the vortex motions and the far-field sound radiation are discussed.

In the presence of a porous material with a finite flow resistance, longitudinal and transverse dipoles coexist in the far field but the latter is significantly weaker than the former in general. When a single vortex engages the porous half-cylinder, the time variation of the strength of each dipole is pulselike. The larger vortex height above the rigid plane reduces the amplitudes of the dipoles. However, the overall acoustical energy radiated remains higher than that in the rigid cylinder case at some combinations of the effective fluid density and flow resistance.

When two identical vortices exist in the proximity of the porous cylinder, both the longitudinal and transverse dipoles consist of a rapidly and a slowly varying frequency components. The former is due to the leapfrogging motions of the vortices, and the latter to the macroscopic vortex centroid motions. The overall acoustical energy so radiated is less than that in the rigid cylinder case when the two vortices are close to each other and the dipoles are dominated by the fast variation fluctuations. The opposite is observed at larger vortex separation.

The present results show that suitable combinations of the effective fluid density and the flow resistance within a porous material will enhance the radiation of sound in the presence of a turbulent shear flow, especially when the flow structures involved are of slow variation frequency.

ACKNOWLEDGMENT

This study was supported by a grant from the Research Grant Council, The Hong Kong Special Administration Region, People's Republic of China (Project No. PolyU5030/00E).

APPENDIX: PARAMETER RANGES FOR EXPERIMENTAL FLOWS

This appendix discusses the ranges of the main parameters of the present study in real flows. The circulation of the vortex in real flow cannot be easily found, but it is believed that such circulation can be approximated by the formula, $\Gamma=(4/\pi)Uh$, shown in Saffman,[33] where U and h are the mean flow speed and the vortex height, respectively. The latter is expected to be close to the turbulent boundary layer thickness δ in a real flow as concluded by Praturi and Brodkey[34] and Robinson.[35] According to Schlichting and Gersten,[36] δ is related to a Reynolds number Re_l as

$$\frac{U\delta}{\nu}=0.14\frac{\mathrm{Re}_l}{\log_e(\mathrm{Re}_l)}G(\mathrm{Re}_l), \tag{A1}$$

where $\mathrm{Re}_l=Ul/\nu$ (l is the distance from the leading edge of the boundary layer and ν the kinematic viscosity of air) and G is a function whose value depends on Re_x. $G\approx1.5$ for $10^5<\mathrm{Re}_l<10^6$ and is equal to 1 as $\mathrm{Re}_l\to\infty$.[36]

Inside a building, the location of silencer has to be far away from flow discontinuity and bends so that the flow is fully developed before it reaches the silencer. It is not diffi-

cult to find $l=10$ m with $U=40$ m/s, giving a $\mathrm{Re}_l \sim 2\times 10^7$. Assume $G\sim 1$, $\delta=6.7$ cm giving $\Gamma=(4/\pi)U\delta=3.4$ m^2/s. Table I summarizes the parameter ranges in practical and experimental flows observed, where use has been made of Refs. 19, 20, and 23 to 27.

One should also note that the fire regulation requires fire dampers to be installed in front of a silencer at the air outlet of the air handling unit.[37] The vortex strength in such a case can be large as the turbulent flow may not be parallel to the damper blades, causing R_f to drop below unity. In the present study, the analysis is focused on the range $R_f \geqslant 1$ and $R_f=0$ (the inviscid fluid case).

[1] M. L. Munjal, *Acoustics of Ducts and Mufflers* (Wiley, New York, 1987).
[2] M. J. Lighthill, "On sound generated aerodynamically I. General theory," Proc. R. Soc. London, Ser. A **211**, 564–587 (1952).
[3] N. Curle, "The influence of solid boundaries upon aerodynamic sound," Proc. R. Soc. London, Ser. A **231**, 505–514 (1955).
[4] L. L. Beranek and I. L. Vér, *Noise and Vibration Control Engineering, Principles and Applications* (Wiley, New York, 1992).
[5] M. S. Howe, *Theory of Vortex Sound* (Cambridge University Press, Cambridge, UK, 2003).
[6] A. Cummings and I. J. Chang, "Sound attenuation of a finite length dissipative flow duct silencer with internal mean flow in the absorbent," J. Sound Vib. **127**, 1–17 (1988).
[7] M. C. Quinn and M. S. Howe, "On the production and absorption of sound by lossless liners in the presence of mean flow," J. Sound Vib. **97**, 1–9 (1984).
[8] K. S. Peat and K. L. Rathi, "A finite element analysis of the convected acoustic wave motion in dissipative silencers," J. Sound Vib. **184**, 529–545 (1995).
[9] J. E. Ffowcs Williams, "The acoustics of turbulence near sound-absorbent liners," J. Fluid Mech. **51**, 737–749 (1972).
[10] S. K. Tang and C. K. Lau, "Vortex sound in the presence of a wedge with inhomogeneous surface flow impedance," J. Sound Vib. **281**, 1077–1091 (2005).
[11] D. G. Crighton, "Radiation from vortex filament motion near a half plane," J. Fluid Mech. **51**, 357–362 (1972).
[12] S. K. Tang, "Effects of porous boundaries on the dynamics of an inviscid vortex filament," Q. J. Mech. Appl. Math. **51**, 65–84 (2001).
[13] F. Obermeier, "New representation of aeroacoustic source distribution. 2. 2-dimensional model flows," Acustica **42**, 62–71 (1979).
[14] P. M. Morse and K. U. Ingard, *Theoretical Acoustics* (McGraw–Hill, New York, 1968).
[15] J. B. Schneider, C. L. Wagner, and R. J. Kruhlak, "Simple conformal methods for finite-difference time-domain modeling of pressure-release surfaces," J. Acoust. Soc. Am. **104**, 3219–3226 (1998).
[16] R. V. Churchill and J. W. Brown, *Complex Variables and Applications* (McGraw–Hill, New York, 1990).
[17] E. J. Routh, "Some applications of conjugate functions," Proc. London Math. Soc. 12, 73–89 (1881).
[18] I. S. Gradshteyn, I. M. Ryzhik, and A. Jeffrey, *Tables of Integrals, Series and Products* (Academic, Boston, 1994).
[19] A. Cummings and N. Sormaz, "Acoustic attenuation in dissipative splitter silencers containing mean fluid flow," J. Sound Vib. **168**, 209–227 (1993).
[20] R. Kirby, "Simplified techniques for predicting the transmission loss of a circular dissipative silencer," J. Sound Vib. **243**, 403–426 (2001).
[21] M. Abramowitz and I. A. Stegun, *Handbook of Mathematical Functions with Formulas, Graphs, and Mathematical Tables* (Wiley, New York, 1972).
[22] H. Abou-Hussein, A. DeBenedictis, N. Harrison, M. Kim, M. A. Rodrigues, F. Zagadou, and M. S. Howe, "Vortex-surface interaction noise: A compendium of worked examples," J. Sound Vib. **252**, 883–918 (2002).
[23] M. E. Delany and E. N. Bazley, "Acoustical properties of fibrous absorbent materials," Appl. Acoust. **3**, 105–116 (1970).
[24] *Rectangular and Cross-Talk Silencers* (Acoustic Engineering Services, Ltd., Surrey, UK).
[25] J. Jimenez, "A spanwise structure in the plane shear layer," J. Fluid Mech. **132**, 319–336 (1983).
[26] K. B. M. Q. Zaman and A. K. M. F. Hussain, "Vortex pairing in a circular jet under controlled excitation. 1. General jet response," J. Fluid Mech. **101**, 449–492 (1980).
[27] Y. Aurégan, A. Debray, and R. Starobinski, "Low-frequency sound propagation in a cylindrical duct: Application to sudden area expansions and to dissipative silencers," J. Sound Vib. **243**, 461–473 (2001).
[28] T. Minota and T. Kambe, "Acoustic-waves emitted by a vortex ring passing near a circular cylinder," J. Sound Vib. **119**, 509–528 (1987).
[29] S. K. Tang and N. W. M. Ko, "Sound sources in the interactions of two inviscid two-dimensional vortex pairs," J. Fluid Mech. **419**, 177–201 (2000).
[30] S. K. Tang and N. W. M. Ko, "Basic sound generation mechanisms in inviscid vortex interactions at low Mach number," J. Sound Vib. **262**, 87–115 (2003).
[31] A. K. M. F. Hussain and K. B. M. Q. Zaman, "An experimental study of organized motions in the turbulent plane mixing layer," J. Fluid Mech. **159**, 85–104 (1985).
[32] J. E. Ffowcs Williams and D. J. Lovely, "Sound radiation into uniformly flowing fluid by compact surface vibration," J. Fluid Mech. **71**, 689–700 (1975).
[33] P. G. Saffman, *Vortex Dynamics* (Cambridge University Press, Cambridge, UK, 1992).
[34] A. K. Praturi and R. S. Brodkey, "A stereoscopic visual study of coherent structures in a turbulent shear flow," J. Fluid Mech. **89**, 251–272 (1978).
[35] S. K. Robinson, "Coherent motions in the turbulent boundary layer," Annu. Rev. Fluid Mech. **23**, 601–639 (1991).
[36] H. Schlichting and K. Gersten, *Boundary Layer Theory* (Springer, London, 2000).
[37] A. E. Cote, *Fire Protection Handbook*, 18th Ed. (National Fire Protection Association, Qunicy, MA1997).